FLORE
Repository istituzionale dell'Università degli Studi di Firenze

Design guidelines for H-Darrieus wind turbines: Optimization of the annual energy yield

(Article begins on next page)

22 December 2024

1 # Design guidelines for H-Darrieus wind turbines: optimization of

2 # the annual energy yield

3 **Alessandro BIANCHINI[1a], Giovanni FERRARA[1b], Lorenzo FERRARI[2c*]**

4 [1] Department of Industrial Engineering, University of Florence

5 Via di Santa Marta 3, 50139, Florence, Italy

6 Phone +39 055 4796 570 - Fax +39 055 4796 342

7

8 [2] CNR-ICCOM, National Research Council of Italy

9 Via Madonna del Piano 10, 50019, Sesto Fiorentino, Italy

10 * Phone +39 055 5225 218 - Fax +39 055 5225 203

11

12 ## Abstract

13 H-Darrieus wind turbines are gaining popularity in the wind energy market, particularly as

14 they are thought to represent a suitable solution even in unconventional installation areas. To

15 promote the diffusion of this technology, industrial manufacturers are continuously proposing

16 new and appealing exterior solutions, coupled with tempting rated-power offers. The actual

17 operating conditions of a rotor over a year can be, however, very different from the nominal

18 one and strictly dependent on the features of the installation site.

19 Based on these considerations, a turbine optimization oriented to maximize the annual energy

20 yield, instead of the maximum power, is thought to represent a more interesting solution. With

21 this goal in mind, 21600 test cases of H-Darrieus rotors were compared on the basis of their

22 energy-yield capabilities for different annual wind distributions in terms of average speed.

a) bianchini@vega.de.unifi.it
b) ferrara@vega.de.unifi.it
c) lorenzo.ferrari@iccom.cnr.it (corresponding author)

The wind distributions were combined with the predicted performance maps of the rotors obtained with a specifically developed numerical code based on a Blade Element Momentum (BEM) approach. The influence on turbine performance of the cut-in speed was accounted for, as well as the limitations due to structural loads (i.e. maximum rotational speed and maximum wind velocity). The analysis, carried out in terms of dimensionless parameters, highlighted the aerodynamic configurations able to ensure the largest annual energy yield for each wind distribution and set of aerodynamic constraints.

Keywords

Darrieus, VAWT, wind turbine, design, energy yield, aerodynamics

1. Introduction

In 2011, the wind energy market grew by 6% compared to 2010, despite the economic and political turmoil in Europe and North America, with a newly installed power of 40.5 GW [1].

The great bulk of installed wind energy plant is today in the form of large wind farms [2] which mainly comprehend large Horizontal Axis Wind Turbines (HAWTs) feeding into power supply grids: turbines are becoming more and more efficient and a scale-up tendency is clearly distinguishable. Moreover, technological improvements in design and efficient maintenance have considerably reduced their operating cost and consequently disclosed new diffusion frontiers like the offshore applications [3-4]. Whereas these installations are a valuable addition to the grid capacity, they actually do not benefit people who are not served by grids. As a consequence, much interest is being paid to understand where wind turbines can effectively represent an alternative for delocalized power production [5-6]. Paradoxically, however, there has been very little research and commercial development in the second part of the century on small stand-alone systems, although great improvements in the blade aerodynamic design have been made. In recent times, a reversal of this trend has been fortunately experienced.

2

47   Increasing interest is especially being paid by architects, project developers and local

48   governments to understand where small wind turbines can effectively be exploited to provide

49   delocalized power in the built environment (e.g. see Refs. [7-12]). The real feasibility of this

50   scenario has, however, yet to be proved, both in terms of real energy harvesting and of

51   compatibility of the machines with a populated area [9-10,13].

52   In particular, Vertical-Axis Wind Turbines (VAWTs), both drag [14-16] and lift-driven [17-

53   20], are gaining popularity in the wind energy scenario, especially in medium and small-size

54   installations, where they can work effectively even in presence of low-speed and unstructured

55   flows with low noise emissions and high reliability. Among others, H-Darrieus rotors are

56   increasingly appreciated in unconventional contexts as they are even assumed to increase their

57   performance in case of an oncoming flow misaligned with respect to the axis of the rotor [17-

58   19]. In order to promote the diffusion of this technology, on one hand, industrial manufacturers

59   are developing new and more appealing design solutions (e.g. [21-25]); on the other hand,

60   efforts are being devoted to reducing the initial cost of the machines (primarily by means of

61   new materials) and to increasing the efficiency, in order to make them competitive with respect

62   to more conventional Horizontal Axis Wind Turbines (HAWTs) [20].

63   Focusing on the commercial aspects, it is also worth pointing out that almost all the industrial

64   rotors are generally designed and optimized for a specific wind speed (i.e. the speed which

65   ensures the highest energy production), but the rated power values, which are often perceived

66   by the final customer as the most valuable indicator of the quality of the product, are declared

67   for their nominal wind velocity, i.e. the highest functioning speed, which provides the

68   maximum power production. Although the importance of accounting for energy instead of

69   power does not come as a surprise for the applied-energy technicians, the implications of this

70   theoretical dichotomy are quite often not completely understood by the final customer of small

71   and medium wind turbines.

72   In detail, the actual operating conditions of a rotor over a year can indeed be very far from the

73   nominal one [9-10,26]. In particular, the available wind energy can be concentrated at the lower

74   wind velocities of the yearly distribution in the installation site, which can be often correctly

75   approximated by a Weibull function [27-30]; in addition, the specific features of the final

76   environment (e.g. local accelerations, effects of obstacles, etc.) are very important in

77   determining the real characteristics of the flow which effectively invests the rotor (e.g. [9-10]).

78   As a result, a turbine optimized only for a singular wind speed could provide poor performance

79   during the largest part of its operating time, with a remarkable reduction of the energy

80   produced and, consequently, of the suitability of the investment [10].

81   Stated the above, a design approach based on the maximization of the annual energy-yield

82   (i.e. the sum of the energy contributions at all the wind speeds experienced over the year) was

83   thought to represent a more valuable solution.

2. Energy-yield-based design strategy

85   The main goal of this study was to define some effective design guidelines for Darrieus wind

86   turbines which would be able to ensure the maximum energy harvesting in a yearly horizon as

87   a function of the attended wind distribution in the installation site.

88   With this goal in mind, 21600 test cases, i.e. permutations of a specific geometrical

89   configuration (300 cases), an airfoil (4 selections), a wind distribution (6 cases) and a load

90   system (3 cases), were tested and analyzed by means of a specifically developed numerical

91   code based on an advanced BEM method, in order to highlight the configurations which ensure

92   the largest annual energy yield for each wind condition.

2.1 Wind distributions

94   As a first step of the analysis, six annual wind profiles were hypothesized. As discussed, the

95   most logical representation of the annual wind distribution must be based on the assumption of

96   a Weibull distribution [27-30]. In particular, in the present study a constant shape factor equal

97   to 2.0 (Rayleigh distribution) was considered, whereas the scale factor was modified in each

98   case in order to ensure an average wind speed ($\bar{U}$) increasing by one from 3 to 8 m/s.

99   The choice of the Rayleigh distribution was based on literature data [9-10], which found that

100   this particular Weibull curve nicely approximates the wind distributions of some medium-low

101   velocity sites in Europe. The presented method, however, is of general validity and can be

102   applied to any Weibull distribution attended in the installation site.

103   In further detail, the wind profiles investigated in this study are shown in Figure 1, where the

104   cut-in and the cut-out limits are also displayed. In particular, it is worth pointing out that a

105   maximum cut-out velocity of 18 m/s was imposed for safety reasons to all the tested rotors

106   [26], based on the industrial experience for these rotors. On the other hand, the cut-in speed

107   was specifically calculated for each rotor on the basis of its behavior at low wind speeds: as

108   shown by Figure 1, a variable cut-in speed between 2 and 3 m/s was measured in the tested

109   rotors. In particular, it is worth pointing out that in the present study the attention was focused

110   only on the Darrieus machines, evaluating their actual self-starting characteristics. Although

111   recent studies (e.g. [31-32]) showed indeed that the self-starting can be enhanced by coupling

112   these rotors with drag-driven devices, the matching of the two turbines was not considered in

113   the scope of the present work and destined to further studies.

114   **2.2 Main design parameters for Darrieus-type turbines**

115   The proper set of rotor configurations to be analyzed was then defined. Due to the large

116   number of variables involved in the aerodynamic design of Darrieus rotors [20,26], some

117   preliminary assumptions were needed to focus the analysis on a significant family of turbines.

118   In particular, the following main choices were made:

119   ▪ The H-Darrieus configuration with straight blades was selected (see Figure 2). This turbine

120   shape is presently the most exploited and studied solution in Darrieus turbines design, due

121   to higher efficiency and lower manufacturing costs with respect to original troposkien-

122   bladed rotors [20,24,33].

123   ▪ A blades number $N=3$ was assumed. This turbine's architecture guarantees a good

124   efficiency and a sufficiently flat torque profile during revolution, without compromising

125   solidity [20,23-24].

126   ▪ At least two supporting struts for each blade were applied (the number was increased by

127   one strut for each blade whenever too high structural stresses were calculated) [21,26].

128   On these bases, the resulting performance maps must be related only to this typology of rotors

129   and future works will be devoted at extending the validity range of the analyses.

130   Then, some significant design parameters to be investigated were chosen [26]. In order to

131   define a set of parameters able to provide a prompt description of the geometrical proportions

132   of the rotor, the attention was focused on:

133   ▪ The *height/diameter ratio* ($\Phi=H/D$);

134   ▪ The *chord/diameter ratio* ($\xi=c/D$);

135   ▪ The *swept area* of the rotor (A);

136   ▪ The airfoil type;

137   ▪ The struts dimensions.

138   In order to understand the aerodynamic implications of these parameters, one has to focus on

139   the physical functioning of Darrieus rotors. In particular, if it is generally well understood that a

140   rotational axis perpendicular to the flow actually results in a flow incidence continuously

141   variable during the revolution, the influence of the chord-based Reynolds number on the

142   airfoils (Eq.1) is generally underestimated, especially in small and medium rotors.

143
$$\mathrm{Re}_c = \frac{wc}{v} \tag{1}$$

144   In further details, when small-sized rotors are designed, the Reynolds number can be very low

145   (especially in case of low wind speeds), even lower than 10^5, being therefore very critical for a

146   correct airfoil functioning.

147   A suitable Re_c on the blade can be achieved through different ways. Assuming that the wind

148   speed cannot be altered (i.e. a specific wind speed is analyzed), the most intuitive solution

149 would consist in a direct increase of the chord c (Eq. 1). This solution is definitely able to

150 accomplish the goal, but strict limitations to its use must be introduced. In particular, notably

151 longer chords produce both a reduction of the Aspect Ratio of the blade (i.e. the ratio between

152 the blade length and the chord - Eq. 2) and an increase of the solidity of the rotor (Eq. 3)

153 [21,24,26].

154
$$AR_b = \frac{H}{c} \tag{2}$$

155
$$\sigma = \frac{Nc}{D} \tag{3}$$

156 The first effect actually results in a detriment of the blade efficiency [18,21], as the increase

157 of the rotor's height to compensate cannot be always provided as the swept area of the rotor is

158 generally a priori selected (Eq.4 for an H-Darrieus).

159
$$A = H \cdot D \tag{4}$$

160 On the other hand, an increase of the solidity also produces a reduction of the peak efficiency

161 of the rotor [20,21,24], which once more cannot be simply compensated by reducing the

162 diameter because this countermeasure would directly reduce the peripheral speed, thus leading

163 to an undesired reduction of the relative speed W (given by the vector sum of the peripheral

164 speed and the wind speed reduced by the induction factor a - see Eq.5):

165
$$W = \omega R + U(1-a) \tag{5}$$

166 The second way to control the Reynolds number on the blade is in fact the modification of the

167 relative speed. Having assumed that the wind speed U is fixed, the only way to modify w is

168 related to a variation of the peripheral speed ωR.

169 Analogous to the previous analysis a double choice is given. An increase of the turbine radius

170 would directly improve the Reynolds number: being A fixed, the turbine's height would be

171 reduced (Eq. 4) and then the Aspect Ratio of the blades (Eq.2), leading to less efficient blades.

172 On the other hand, increasing the revolution speed would improve the relative speed, having,

173   however, a notable impact on the incidence angles range and the structural behavior of the

174   rotor.

175   Based on the above, the influence of the selected parameters can be readily highlighted.

176   ▪ ***Φ ratio*** - The Φ ratio has a double effect in defining the features of the rotor. From an

177   aesthetic point-of-view, it can be considered as a "shape factor" of the turbine, i.e. an

178   indicator of the visual proportions of the virtual cylinder swept during the revolution. On

179   the other hand, for a fixed swept area, low Φ values are typical of a machine in which the

180   optimal flow conditions on the airfoil are obtained thanks to large diameters in order to

181   increase the peripheral speed. In this configuration, the velocity triangles on the airfoils are

182   improved but the blades are generally short, with more relevant losses due to end-effects.

183   Conversely, high Φ values can be related to machines in which the efficiency of the blade

184   (high blade Aspect Ratios - Eq. 2) is preferred.

185   ▪ ***ξ ratio*** - The c/D ratio is a direct indicator of the solidity (σ) of the rotor (Eq. 3). High

186   values of ξ generally indicate that the chord length is increased to improve the Reynolds

187   number, whereas low ξ values can be related to rotors in which the relative wind speed is

188   increased by means of an increase of the relative wind speed on the airfoil (Eq. 5).

189   ▪ ***Swept Area (A)*** - As one can argue from the previous discussion, the swept area of the

190   turbine (Eq. 4 - valid for an H-Darrieus rotor) is unfortunately a dimensional parameter

191   which cannot be bypassed in the analysis of small rotors. In particular, larger swept areas

192   ensure less demanding limits of the turbine's radius, ensuring higher peripheral speed and,

193   therefore, fewer problems in ensuring a good Reynolds number on the blades. Moreover,

194   being the optimal solidity ranges generally constant [20-21], the minimum requested

195   chords are generally smaller, resulting in higher Aspect Ratios and more efficient blades.

196   ▪ ***Design variables*** - The airfoil type is very important in defining the performance of a

197   Darrieus turbine; as a result, the dimensionless analysis on the best design trends must be

198   individually carried out for each specific airfoil family [20,34-35]. Finally, the struts'

8

199   shape and dimensions must be carefully taken into account as they can substantially

200   modify the power output of an H-Darrieus rotor (see Refs. [21,24,33,36]) due to the

201   parasitic torque that is produced during the revolution. To this purpose, the impact of the

202   struts was also included in this study by assuming a variation of their dimensions, and even

203   number, as a function of the structural stresses on the blades.

204   **3. Test plan and design parameters**

205   The test plan of the investigated configurations is summarized in Table 1.

206   The limits of the ξ and Φ parameters were defined on the basis of a survey of the technical

207 literature (e.g. [5,20,24]). In particular, the ξ range was limited to 0.200 as higher values would

208 lead to solidities higher than 0.6. Design choices over this limit are in fact considered to be

209 unsuitable for H-Darrieus rotors [20,24], due to the fact that the turbine is deemed to become

210 similar to a solid obstacle for the wind and the interactions between upwind and downwind

211 blades becomes so strong to compromise the aerodynamics of the airfoils. In addition, the

212 theory applied in the simulations could become less predictive in similar test-cases [20].

213   The choice of the aerodynamic airfoils was also based on a literature survey [5,20-21]. In

214 particular, four different airfoils were investigated in this work, in order to highlight the impact

215 of their aerodynamic characteristics on the effective energy harvesting of the turbine. The

216 airfoils were selected among the 4-digit NACA family, which is quite a conventional solution

217 in Darrieus VAWTs [5,20,34-35].

218   In detail, three uncambered airfoils with different thickness/chord ratios (NACA0012,

219 NACA0015, NACA0018) were compared to an asymmetrical and lightly-cambered airfoil

220 (NACA4415). The first group of airfoils is a widely exploited solution in Darrieus turbines, as

221 it ensures a suitable resistance to the stall coupled with good lift outputs at medium-range

222 Reynolds numbers. Moreover, a symmetric airfoil is able to provide the same lift contribution

223 either with positive or negative incidence [20,24]. On the other hand, a cambered profile, like

224 the selected NACA4415, has been suggested in technical literature (e.g. see [5,21]) as an

225   interesting design choice in order to ensure high peak values of the torque in low-velocity

226   cases, although some doubts on their effective application are due to the different behaviour of

227   a non-symmetric airfoil in case of a positive or negative incidence [21].

228   Focusing on the boundary conditions in terms of loads applied to the rotor, three different

229   configurations were analyzed:

230   ▪ **CASE 1 – Aerodynamics only**: in this configuration, the contribution of the resistant

231   torque of the struts was not considered. By doing so, this configuration actually refers to a

232   hypothetical solution of a fully aerodynamic relationship between the geometrical features

233   of the rotor and the power performance. Although not practically applicable, the analysis

234   of these results allows one to define the aerodynamic trends and to directly compare the

235   functioning behavior of machines having different areas. Moreover, by defining the purely

236   aerodynamic requests, one can also directly identify the effects induced by the secondary

237   and parasitic effects due to auxiliary organs (e.g. the struts) and external loads.

238   ▪ **CASE 2 – Centrifugal load**: the contribution of the resistant torque of the struts was again

239   not considered but a limitation on the centrifugal stress acting on the blades was added as a

240   function of the rotational speed of each model.

241   ▪ **CASE 3 – Struts' parasitic torque**: in this latter configuration, both a limitation on the

242   centrifugal stress on the blades and variable struts dimensions, as a function of the

243   rotational speed of each model, were included. Moreover, the resistant torque of the struts

244   was taken into account.

245   In order to give a correct estimation of the structural loads, in this study a manufacturing

246   technology based on extruded aluminium blades with a hollowed section was considered,

247   utilizing real data on both the maximum centrifugal stress and on the maximum mechanical

248   stress on the struts available from previous design experiences of the authors [33].

249   In further detail, in Case 2 the cut-out speed of the turbine was calculated in each case-study

250   based on the hypothesis that the maximum centrifugal stress at the middle of the blade (where

251   the maximum displacement is located) would not exceed a fixed stress limit of the blade itself

252   (Eq. 6).

253

$$\varsigma_b = \frac{F_b}{A_{res\_b}} = \frac{m_b \omega^2 R}{A_{res\_b}} \leq \varsigma_{\lim\_b} \tag{6}$$

254   where A_{res_b} is a conventional resistance area which takes into account the structure of the

255   stiffeners inside the airfoil and F_b is the centrifugal stress of the blade of mass m_b. In particular,

256   all the airfoils were reproduced with a hollowed section having a constant skin thickness (3

257   mm) and three, equally spaced, rectangular stiffeners perpendicular to the chord of variable

258   thickness. The trailing edge was considered as solid with a filet radius increasing proportionally

259   to the chord of the blade (Figure 3). Based on the characteristics of an aluminium alloy tested

260   by the authors in a previous industrial experience [33,37], a stress limit of 90 N/mm^2 was here

261   considered.

262   In addition, in Case 3 even the dimensions of the struts (at least two for each blade) are

263   variable from one configuration to another in order to satisfy the stress limit of the blades due

264   to the centrifugal force (Eq. 7 with the same notation of Eq. 6).

265

$$\varsigma_{ST} = \frac{F_{ST}}{A_{res\_ST}} = \frac{1}{N_{ST}} \frac{m_b \omega^2 R}{A_{res\_ST}} \leq \varsigma_{\lim\_ST} \tag{7}$$

266   It is worth pointing out that the load case considered in Eq. 7 takes into account only the

267   tensile stresses generated by the centripetal acceleration of the rotor. In authors' experience

268   (see [33,37]), this load condition is quite realistic for small-size rotors (i.e. with a swept area up

269   to 4.0 m^2), whereas bending forces become significant in larger rotors with high Φ ratios. In

270   this work, the bending stresses were neglected but a more accurate description of their

271   influence will be carried out in future works.

272   A correct evaluation of the strut's dimensions is particularly important in small rotors due to

273   the fact that a fast-rotating turbine often needs thick supporting struts to balance the centrifugal

274 stresses [24]. Similar struts, however, are characterized by a notable parasitic torque generation

275 which causes a remarkable detriment of the overall performance of the machine.

276   In particular, in this study a constant shape of the struts was considered. In case of

277 symmetrical airfoils, the same profiles were used. On the other hand, when the NACA4415 is

278 used, the struts are supposed to be realized with the NACA0015 (same t/c ratio but straight

279 camber). By these choices, a constant virtual drag coefficient [24] during the revolution was

280 considered, whereas the dimensions of the struts were varied in Case 3 until the minimum ones

281 which satisfied Eq. 7 were found. In detail, the chord of the struts (and consequently also the

282 thickness, being the t/c ratio fixed) was calculated on the basis of the resistant area defined by

283 Eq.7. When the calculated struts dimensions exceeded the chord of the blade, the struts number

284 was increased by one for each blade and the new dimensions of each element were re-

285 calculated on the basis of the same procedure, in all the investigated configuration, a maximum

286 struts' number of three was constantly observed. Finally, the effects of "bluff-section" struts

287 was investigated, in order to stress more evidently the influence of the parasitic phenomena: the

288 struts were assumed to have a constant virtual drag of 0.3 and a thickness varying with the

289 same procedure described for the airfoil-shaped solutions.

4. Simulations and data reduction

291   The performance simulations of the machines were carried out with the *VARDAR* code of the

292 Department of Industrial Engineering of the University of Florence. The code makes use of the

293 Blade Element Momentum (BEM) Theory, by which the rotor performance is calculated

294 coupling the momentum equation in the mainstream direction of the wind and a one-

295 dimensional aerodynamic analysis of the interactions between the airfoils in motion and the

296 oncoming flow on the rotor [20,33,38-39] by means of pre-calculated polars. Even if more

297 advanced simulations techniques (including computational fluid dynamics) are today available

298 for the simulation of VAWTs (e.g. [39-41]), BEM approaches are still the most widely

299 exploited tools for the preliminary design of these rotors, as they provide sufficiently reliable

300 results in terms of global performance (whereas a poor description of the instantaneous flow

301 field around the rotor is achieved) coupled with a notably reduced computational cost.

302 In particular, the VARDAR code has been specifically developed for H-Darrieus wind

303 turbines using an improved version of a *Double Multiple Streamtubes Approach with Variable*

304 *Interference Factors* [17,28,42] (Figure 4a). In this approach, the elementary torque for each

305 azimuthal position is therefore given by Eq. 8:

$$T_{blade}(\vartheta) = F_t \cdot R = \frac{1}{2}\rho c W_\vartheta{}^2 C_{t(\vartheta)}RH \tag{8}$$

306

307 where C_t and W represent the tangential coefficient of the airfoil in the reference system of the

308 rotating blade (Figure 4b) and the relative velocity of the flow experienced by the airfoil itself

309 in the upwind or downwind half, respectively, expressed by Eqs. 9,10 and 11:

$$C_t = C_L \cdot \sin\alpha - C_D \cdot \cos\alpha \tag{9}$$

310

$$W_{up} = \sqrt{\left[(1-a)\cdot U_\infty \cdot \sin(\vartheta - \beta)\right]^2 + \left[(1-a)\cdot U_\infty \cos(\vartheta - \beta) + \omega R\right]^2} \tag{10}$$

311

$$W_{down} = \sqrt{\left[(1-a_2)\cdot U_{eq} \cdot \sin(\vartheta - \beta)\right]^2 + \left[(1-a_2)\cdot U_{eq} \cos(\vartheta - \beta) + \omega R\right]^2} \tag{11}$$

312

313 As for the more general Eq. 5, the relative speed is given by the sum of peripheral speed and

314 wind speed, properly reduced by the induction factor (either upwind or downwind). The value

315 U_{eq} in Eq. 25 indeed represents the wind equilibrium velocity between actuator disks (see

316 Figure 4).

317 The Glauert's correction for the BEM theory has been taken into account with the most recent

318 improvements, together with the corrections due to blades finite Aspect Ratio, using the

319 Lanchester-Prandtl model. This aspect is of particular relevance in the present analysis, as it

320 allows the designer to account for the increasing tip-losses connected to blades with small

321 height to chord ratios.

322 In order to increase the accuracy of the aerodynamic estimations, a specific sub model to

323 account for the dynamic stall has been provided, following the Paraschivoiu's adaptation to the

324 DMS approach described in; at the same time, the stream tube expansion along the flow path

325 was considered. For additional details on the code please refer to Refs. [23,26,33,37,42-43].

326　 The prediction capabilities of the VARDAR code have been validated during a several-years'

327 experience in the design of three real H-Darrieus rotors, having swept areas of 1, 2.5 and 5 m^2,

328 respectively, and two or three blades, either straight or helix-shaped. The 1:1 models of all the

329 rotors (two made of reinforce plastic and one of painted aluminium alloy) were tested in

330 different wind tunnels (both with closed and open-jet). In all cases, the code was able to

331 correctly predict both the power curves at different wind speeds and the starting ramps of rotor

332 and is then considered fully predictive for the turbine typology investigated in this study. For

333 further details on the code validation please refer to Refs. [23,33,37,42].

334　 In the present analysis, the code provided the power coefficient of each configuration at all

335 the wind speeds between the cut-in and the cut-out. The characteristic power coefficient of the

336 machines at each wind velocity was conservatively evaluated in correspondence with the

337 calculated performance 0.2 points of TSR after the peak of the operating curve. A similar

338 precaution is often applied in order to define a load curve aimed at preventing the turbine from

339 operating in the unstable part of the functioning curve [11,24]. Moreover, it is worth noticing

340 that the cut-in speed in each case was set to the wind speed for which a positive power

341 coefficient is obtained. This is, in fact, a precautionary assumption, because the self-starting of

342 an H-Darrieus rotor in real wind is often ensured for several starting positions even if the

343 overall power coefficient over the revolution is negative [42,45].

344　 In further detail, for each configuration in terms of swept area (i.e. the discrete variable of the

345 problem) specific performance maps were created [26] corresponding to a given wind

346 distribution. Each map (e.g. see Figure 5) contains the overall efficiency of energy conversion

347 (η_{en}) of the specific rotor, defined as in Eq. 12 and 13.

348
$$\eta_{en} = \frac{\sum\limits_{u=cut-in}^{cut-out} c_P(u) \cdot u^3 \cdot T(u)}{\sum\limits_{u=cut-in}^{cut-out} u^3 \cdot T(u)} \tag{12}$$

14

$$T(u) = f(u) \cdot 8760 \qquad (13)$$

349

350   Upon examination of the equations, it is worth pointing out that the energy conversion

351   efficiency was defined as the annual energy yield of the turbine over the year (i.e. the real

352   extracted power at each wind speed multiplied by the time fraction, in hours, during which that

353   wind blows $T(u)$) on the theoretical energy contained in the wind itself.

354   Based on its definition, this indicator differs from the classical power coefficient and allows

355   one to simultaneously take into account both the efficiency of the turbine at all the wind speeds

356   expected over the year and the effects related to the starting and resistance capabilities of the

357   rotor (due to the variable cut-in and cut-out velocities considered).

358   Finally, within each map, a numerical identification of the maximum was performed, with the

359   constraints of neglecting design solutions which imply Blade's Aspect Ratios higher than 35: in

360   case of excessive ratios between the height and the chord, the bending resistance of such a

361   slender blade would be indeed very poor, making the selected solution practically unfeasible.

362   This procedure would finally lead to the definition of the geometrical features of the rotor

363   ensuring the largest energy harvesting over a year for the attended load case, average wind

364   speed in the site and imposed swept area of the rotor.

365   The whole data reduction procedure is summarized in Figure 6, while a complete overview on

366   the results in terms of best design solutions can be find in the Appendix Section.

5. Results

367

5.1 Energy Efficiency maps interpretation

368

369   A typical Energy Efficiency map has been presented in Figure 5 (e.g. for a swept area of 4.0

370   m², NACA0018 airfoil, $\bar{U}$=5 m/s in Case 2). A linear interpolation was performed between the

371   calculated points (see Table 1) in order to more precisely outline the contours.

372   It is readily noticeable that an optimum-design zone (white-colored in the figure) can be

373   typically distinguished in the bottom side. This zone represents the combination of the Φ and ξ

15

374 parameters which ensures the best compromise in terms of functioning Reynolds numbers on

375 the airfoil (high peripheral speeds and chords) and efficiency of the blades (high Aspect

376 Ratios). Moreover, one can also notice that the efficiency is almost zero in the left side of the

377 map, where the very small chords remarkably reduce the lift generation, and becomes lower

378 also in the right-bottom corner of the map, where the turbine heights tend to zero.

379 As discussed, within each map a numerical identification of the maximum was performed in

380 order to define the geometrical features of the rotor ensuring the largest energy harvesting over

381 a year under the present design constraints.

382 **5.2 Case 1 - Aerodynamics**

383 From a general point of view, it is worth remembering that Case 1 configuration actually

384 refers to a hypothetical solution of a fully aerodynamic relationship between the geometrical

385 features of the rotor and the power performance. By doing so, the influence of the main

386 aerodynamic design parameters can be readily argued and the functioning behaviors of

387 machines having different areas can be directly compared.

388 The main outcome of the analysis of Case 1 is that an opposite behavior was found between

389 cambered and uncambered airfoils in this configuration.

390 As an example of uncambered airfoils, Figure 7 reports the variation trends which describe

391 the dependence of the optimal values of the most relevant design parameters from the average

392 wind speed for the NACA0015 airfoil.

393 Upon examination of Figure 7, some relevant markups can be promptly made. In particular:

394 ▪ The dimensionless parameters present the same trends even when different swept areas are

395 considered, although numerical values differ from one configuration to another,

396 confirming that scale effects must be taken into account.

397 ▪ When the average wind speed in the site increases, the best solidity decreases constantly

398 and the Aspect Ratio rises significantly, whereas the Shape Factor Φ increases for

399   medium-low average wind speeds and then becomes stable. As a general remark, however,

400   the turbine tends to become slenderer by increasing the average wind speed.

401   ▪ Focusing on the dimensional parameters, the aforementioned trend is basically obtained

402   throughout a constant decrease of the blades' chord with the average wind speed increase

403   (with a steeper trend for medium-low $\bar{U}$ and a flatter trend with an increased $\bar{U}$). The

404   turbine diameter and height have instead an opposite trend, with a decrease and an increase

405   in the first part, respectively, followed by a constant trend in the second part.

406   The main aerodynamic implication of these results is that, when the average wind velocity

407   experienced by the turbine is low (left side of the plots), the best design is that ensuring the

408   highest local Reynolds numbers on the blade by means of the geometrical proportions. As a

409   consequence, the chord values are maximized (see Eq. 1) at low wind speeds and then the

410   solidity values are high (Eq. 3).

411   By increasing the average wind speed, the velocity triangles on the airfoils are altered thanks

412   to the increased relative velocities experienced by the blades: the chords can be therefore

413   reduced without decreasing the functioning Reynolds numbers. For high mean wind velocities,

414   however, the chord length stops decreasing and more efficient blades (i.e. higher Aspect Ratios,

415   *AR=H/c* [20-21,24]) are obtained by means of an increase of the turbine height (black curves in

416   the graphs on the left). The optimal solidity constantly decreases with $\bar{U}$.

417   Moreover, a well-defined dependence on the *t/c* ratio of the airfoil was observed. For

418   example, in Figures 7 and 8 the optimal trends of the solidity and the blade's Aspect Ratio for

419   the three uncambered airfoils are reported.

420   In detail, by decreasing the *t/c* ratio of the selected airfoil (Figure 8), i.e. from NACA0018 to

421   NACA0015 and NACA0012, the optimal solidity of the turbine is constantly reduced. This

422   phenomenon can be related to a decrease of the requested chord. This solution is indeed

423   allowed by an increase of the target peripheral speed of the rotor which, on one hand, ensure a

424   suitable Reynolds number on the airfoil (Eq.1) and, on the other hand, decreases the incidence

17

angles range: thinner airfoils (e.g. the NACA0012), although more efficient for high relative speeds, have indeed a lower stall angle and are generally more sensitive to incidence angle variations. Contemporarily (Figure 9), the same reasons induce an opposite behavior of the blade's Aspect Ratio (AR_b), which is constantly higher in case of thinner airfoils (the shorter chords are combined with an almost equal trend of optimal heights).

The optimal design trends in case of the cambered NACA4415 airfoil are notably different. In particular, whenever this typology of profile is applied, the scale effects due to the swept area become negligible, as the high C_L/C_D ratio of this airfoil [44] makes the dependence of the aerodynamic performance from the chord very low. The Aspect Ratio can then rise significantly to pursue the higher blade's efficiency. The optimal design proportions in Case 1 for the NACA4415 airfoil are reported in Figure 10. In this configuration, the optimal solidity is low (see Eq. 3) and the AR_b very high mainly due to the very short chords.

5.3 Case 2 - Limited centrifugal load

The results obtained from the examination of Case 1 are very useful to comprehend the aerodynamic trends connected to a variation of the wind velocities experienced by the turbine; structural constraints like the centrifugal load have, however, relevant impact on the best design compromise of a machine [24,26].

To this purpose, next figures report some results of the investigation on the study-cases in Case 2, in which a ς_{lim_b} (Eq. 6) of 90 N/mm^2 was considered [26,33]; for a wider overview of the results, please see Appendix B.

First, it was noticed that, when the average wind velocities are low (i.e. 3÷4 m/s), the structural constraints actually do not affect the definition of the best design parameters; the operating rotational speeds at these velocities are low and the resulting centrifugal loads do not exceed the structural limits. In case of the NACA4415, the best design is once again imposed due to limitation on the blade's Aspect Ratio.

450   Once again, the two types of airfoils work differently. If the uncambered profiles are selected

451   and the medium-high wind speeds become more frequent, the reduction of the solidity with the

452   average wind speed noticed in Case 1 ceases (an almost constant value is reached – e.g. see

453   Figure 11), mainly due to the stop in the decrease of the optimal chord (Figure 12).

454   This trend can be explained by considering that, when the wind velocities are high, the most

455   suitable compromise in terms of energy-yield capabilities comes from a reduction of the peak

456   efficiency of the turbine (higher solidity) which, however, implies a reduction of the operating

457   rotational regime [24,26]. This reduction makes the centrifugal loads decrease and allows the

458   turbine to extract energy from the wind with all the considered wind velocities.

459   In particular, after examining the Energy Efficiency maps (e.g. for the NACA0018, swept

460   area $A=4$ m^2 in Figure 13), it is readily noticeable that, for low average wind speeds, the best

461   efficiency zone first migrates towards lower solidities and higher Φ ratios. When the high wind

462   speeds become more frequent, however, a new zone of best efficiency arises at higher ξ and Φ

463   ratios.

464   On the other hand, in case the NACA4415 is adopted, the optimal design solution highlighted

465   in Case 1 (small chords, very high AR_b and high revolution speeds) is no longer feasible due to

466   the limitation to the centrifugal load.

467   As a result, the best solidity value is slightly increased for medium-high average wind speeds

468   (Figure 14); contemporarily, the chords and diameters remarkably increase in order to achieve

469   a drastic reduction of the revolution speed (Figure 15). One should indeed remember that

470   longer chords ensure more favorable Reynolds numbers on the airfoil without increasing the

471   relative speed (see Eq. 3), whereas higher diameters act oppositely by improving the relative

472   speed (Eq. 4) or, conversely, ensure the same relative speed with lower revolution speeds.

473   Finally, it also worth noticing that this increase of the diameter for high average wind speeds

474   is avoided only for high swept areas (i.e. $A=9.0$ m^2), where the limit on the centrifugal load is

475   mitigated by the large diameters. In these conditions, the AR_b can be also slightly increased,

476   with a partial recovery of the blades' efficiency (see Appendix B).

477   **5.4 Case 3 - Centrifugal load and struts' parasitic torque**

478   Focusing now on a real-type machine, a further constraint must be included in the

479   identification of the best design trends: the parasitic torque of the struts is, in fact, a key

480   element in defining both the peak efficiency of the machine and its functioning behaviour at

481   different wind speeds. Due to the relevance of this load case, the complete comparison of the

482   optimal design configurations was reported in Appendix D.

483   The calculations showed that the general effect of the parasitic torque is to slightly flatten the

484   trends of the design parameters as a function of the average wind speed. The best design

485   solutions tend in fact to collapse in the configurations that minimize the contribution of the

486   parasitic components [26]. The general tendencies described in Section 4.3 are, however, still

487   of validity and will not be all again discussed. In particular, the efficiency maps shape

488   discussed in Figure 13 was confirmed also under this load case, with the only discussed

489   restriction of the high-efficiency zone. Some interesting remarks can however be made.

490   First, Figure 16 reports the comparison between the optimal solidity trends in Case 2 and 3 for

491   NACA0012 and NACA0018 airfoils (swept area of 1.0 m^2), as a function of the average wind

492   speed. As one may notice, no great difference stands between the two cases when the average

493   wind speed in the site is sufficiently high (i.e. higher than 5 m/s). Conversely, in case of low

494   average wind speeds, the optimal solidity in Case 3 is higher than that obtained in case the

495   parasitic torque is neglected.

496   In order to give a correct interpretation of the results, it is worth remembering that the

497   parasitic torque generated by the rotating structures which do not contribute to the torque

498   generation (e.g. struts, tie-rods, etc.), has a quadratic dependence on the rotational speed of the

499   rotor (directly affecting the tangential velocity) and a lighter and more complex dependence on

500   the wind velocity (see Refs. [33,36]).

20

501   Based on these considerations, one can understand that, when the wind speeds are low, the

502   impact of the parasitic torque on the effective energy-extraction capability of the rotor is more

503   relevant: as a consequence, the optimal design tends to increase the solidity, in order to achieve

504   a reduction of the revolution regime [24].

505   Focusing on the cambered airfoil, the situation is again quite different (see Figure 17). With

506   this airfoil selection, which is thought to provide a good torque production even in low winds,

507   the best design solution is almost unaltered within $\bar{U}$=5 m/s with respect to Case 2.

508   When the high wind speeds in the site become more frequent, however, the "low solidity"

509   solutions, which are associated with very high revolution speeds, are not suitable anymore, as

510   the parasitic torque has become too high. The optimal solutions hence tend to higher solidities

511   (i.e. slower revolution speeds), very similar to those identified for the uncambered airfoils.

512   Finally, in order to further stress the importance of the parasite torque of the struts, in Figure

513   18 a comparison between the optimal solidity for a turbine with the NACA0012 airfoil and a

514   swept area of 1 m^2 is reported as a function of the strut's shape. In detail, when the drag of the

515   struts increases, the solidity tends to notably increase, in the attempt of reducing the revolution

516   speed of the rotor. In the selected case, the more energy-efficient solution would be very solid

517   (even up to the limit of $\sigma = 0.6$), which is, however, a practically unfeasible solution. In a

518   similar case, a compromise must be pursued in practically designing the rotor, including a

519   reduction of the effective energy-yield capabilities.

520   At the end of this study, one could then conclude that, from an energy viewpoint, future

521   design of medium and small-size Darrieus rotors should be based on the maximization of the

522   energy yield on the basis of the characteristics of the potential installation site. In particular, for

523   given rotor's dimensions, a differently shaped turbine would be about to be preferred as a

524   function of the average wind speed of the installation. For example, in Figure 19 the optimal

525   design choices for a turbine having a swept area of 4 m^2 and equipped with NACA0018 airfoils

526   are presented as a function of the average wind speed in the site. In particular, the

527   aforementioned trends in terms of increase of the H/D ratio and decrease of the chord length

528   are clearly distinguishable.

529   For the same family of turbines (presented trends are consistent with all the analyses

530   presented in this study), the annual energy yield of the optimized rotors is presented in Figure

531   20 as a function of the average wind speed in the site. In order to provide a sensitivity analysis

532   on the benefits of the proposed approach, in the same figure the energy yield increase with

533   respect to two others design choices is presented. In further details, Study Turbine A represents

534   a hypothetical turbine designed to have the maximum efficiency at 6 m/s, which could be, for

535   example, the average speed in the site [23]. Study Turbine B instead represents the turbine

536   optimized by means of the maximum-energy-yield criterion at $\bar{U}$=6 m/s.

537   Some very interesting remarks can be done. First, it is worth noticing that a design approach

538   based on the maximum annual energy yield actually provides an increase of performance in all

539   cases. In particular, focusing on the 6 m/s bar, one can notice that benefits can be achieved also

540   in comparison to a design criterion based on the same average speed of the site.

541   Moreover, the proposed criterion is able to provide notable energy increase (up to 10% in the

542   present case) when the wind speeds in the site are low, confirming the prospects of specific

543   future design choices for these conditions.

6. Conclusions

545   In this study, a numerical analysis has been carried out to define some design guidelines for

546   Darrieus wind turbines aimed at optimizing the annual energy yield of each machine in the

547   installation site. The main outcomes of the analysis can be summarized as follows.

548   Focusing on the only aerodynamic requirements, an opposite behavior was found between

549   cambered and symmetric, uncambered airfoils. For uncambered profiles, when the average

550   wind speed in the site increases, the best solidity decreases constantly, the Aspect Ratio rises

551   significantly, whereas the Shape Factor Φ increases for medium-low average wind speeds and

552   then becomes stable. This trend is mainly due to the fact that, by increasing the wind speed, the

553 relative velocity is increased, and the Reynolds number is improved. The chords can be then

554 reduced, with notable benefits in terms of blade's efficiency. A well-defined dependence on the

555 *t/c* ratio was also observed: by decreasing the *t/c* ratio, the optimal solidity is constantly lower

556 whereas higher Aspect Ratios are preferable. When a cambered airfoil is instead selected, the

557 scale effects due to the swept area becomes negligible, as the high C_L/C_D ratio of this airfoil

558 makes the dependence of the aerodynamic performance from the chord very low, hence

559 allowing the Aspect Ratio to rise significantly to pursue the higher blade's efficiency. With this

560 selection, the optimal solidity is consequently also very low.

561 On the other hand, when structural constraints and notable parasitic contributions are

562 introduced, the best configurations when the average wind velocities are low are similar to that

563 coming from the aerodynamic analysis, although the optimal design generally tends to increase

564 the solidity, in order to ensure a better functioning conditions to the airfoils (higher Reynolds

565 numbers, increased torque) and contemporarily achieve a reduction of the revolution regime,

566 which contains the parasitic torque. On the other hand, when the medium-high wind speeds

567 become more frequent, the most suitable compromise in terms of energy-yield capabilities

568 generally comes from a reduction of the peak efficiency of the turbine which, however, ensures

569 a good energy extraction is a wider range of functioning conditions. In case of uncambered

570 airfoils, in particular, this goal is obtained with a general increase of the optimal solidity, which

571 makes the revolution speed decrease and allows the turbine to extract energy from the wind

572 with all the considered wind velocities. As a general remark, however, by increasing the

573 parasitic contributions, the transition of the best design compromise to higher solidity solutions

574 is anticipated, due to the stronger dependence of the performance on the rotational speed.

575 At the end of this work, it has to be noticed that the present analysis was carried out under

576 specific assumptions in terms of dimensions, airfoil types, load system and struts' shape; on

577 these bases, the reader has to consider that different performance maps could come from a new

578 set of theoretical assumptions, although some general trends outlined in the work (e.g. the

579   influence of the turbine proportions on the Reynolds numbers and the rotational speed) are of

580   general validity.

581   The proposed design criterion, however, besides being theoretically more rigorous from a

582   truly energetic point-of-view than a conventional one based on a single reference wind speed,

583   has shown interesting prospects in terms of energy production improving. In particular,

584   different models could be designed for specific wind distributions in order to optimize the

585   energy yield also at low wind speeds, which are very frequent in several countries and in

586   unconventional installation sites, e.g. the urban environment.

587   **Nomenclature**

588   A Swept Area $[\text{m}^2]$

589   a Induction Factor

590   AR Aspect Ratio

591   c Blade Chord $[\text{m}]$

592   C_D Drag Coefficient

593   C_L Lift Coefficient

594   C_t Tangential Force Coefficient

595   c_P Power Coefficient

596   D Turbine Diameter $[\text{m}]$

597   F_n Normal Force on the Blade $[\text{N}]$

598   F_{ST} Force due to Centrifugal Loads $[\text{N}]$

599   F_t Tangential Force on the Blade $[\text{N}]$

600   f Frequency

601   H Turbine Height $[\text{m}]$

602   m Mass $[\text{kg}]$

603   N Blades/Struts Number

604   P Power $[\text{W}]$

605	R	Turbine Radius	[m]
606	Re_c	Chord-based Reynolds Number	
607	T	Annual Time of each Wind Class	[h]
608	t	Airfoil Thickness	[m]
609	TSR	Tip-Speed Ratio	
610	u	Wind Class	[m/s]
611	U_∞	Absolute Wind Speed	[m/s]
612	$\bar{U}$	Average Wind Speed	[m/s]
613	W	Relative Wind Speed	[m/s]
614			
615	Superscripts		
616	$*$	Per Unit Area	
617	$\rightarrow$	Vectorial Quantity	
618			
619	Subscripts		
620	air	Air	
621	b	Blade	
622	en	Energy	
623	eq	Equilibrium (between upwind and downwind)	
624	res	Resistant Component	
625	ST	Struts	
626			
627	Greek letters		
628	Φ	Turbine Shape Factor	
629	α	Incidence Angle on the Airfoils	[deg]
630	β	Pitch Angle	[deg]
631	η_{en}	Energy-conversion Efficiency	

632	v	Kinematic Viscosity	$[m^2/s]$
633	ξ	Chord/Diameter Ratio	
634	ρ	Air Density	$[kg/m^3]$
635	σ	Solidity	
636	ς	Structural Stress	$[N/m^2]$
637	ω	Rotational Speed	$[rad/s]$

638 References

639 [1] Global Wind Report. Global Wind Energy Council; 2011.

640 [2] Global Wind Energy Outlook. GWEC, Brussels (Belgium); 2011.

641 [3] Oceans of Opportunity. EWEA, Brussels (Belgium); 2009.

642 [4] Junginger M, Faaij A, Turkenburg WC. Cost Reduction Prospects for Offshore Wind
643 Farms. Wind Engineering 2004;28(1):97–118.

644 [5] Kirke BK, Evaluation of self-starting vertical axis wind turbines for standalone
645 applications. Ph.D. thesis, Griffith University, Gold Coast (Australia); 1998.

646 [6] Small Wind Turbine Global Market Study. AWEA, Whashington DC (USA); 2008.

647 [7] Mertens S. Wind Energy in the Built Environment. Brentwood (UK): Multi-Science; 2006.

648 [8] Dayan E. Wind energy in buildings: Power generation from wind in the urban environment
649 - where it is needed most. Refocus 2006;72(2):33-38.

650 [9] Beller C. Urban Wind Energy - State of the Art 2009, Risø Laboratory - DTU, Roskilde
651 (Denmark), Tech. rep. Risø-R-1668(EN); 2009.

652 [10] Balduzzi F, Bianchini A, Ferrari L. Microeolic turbines in the built environment: influence
653 of the installation site on the potential energy yield. Renewable Energy 2012;45:163-174.

654 [11] Balduzzi F, Bianchini A, Carnevale EA, Ferrari L, Magnani S. Feasibility analysis of a
655 Darrieus vertical-axis wind turbine installation in the rooftop of a building. Applied Energy
656 2012;97:921–929.

26

657 [12] Syngellakis K. Urban wind turbines: Development of the UK market. Proc. of the

658 European Wind Energy Conference 2006, February 27-March 2, Athens (Greece); 2006.

659 [13] Banks D, Cochran B, Denoon R., Wood G. Harvesting Wind Power from Tall Buildings.

660 Proc. of the CTBUH 8th World Congress, Dubai (UAE), 2008 In: Chicago: Council on Tall

661 Buildings and Urban Habitat; 2008, pp. 320-327.

662 [14] Sarma NK, Biswas A, Misra RD. Experimental and computational evaluation of Savonius

663 hydrokinetic turbine for low velocity condition with comparison to Savonius wind turbine at

664 the same input power. Energy Conversion and Management 2014;83:88-98.

665 [15] Roy S, Saha UK. Review of experimental investigations into the design, performance and

666 optimization of the Savonius rotor. Proc. of the Institution of Mechanical Engineers, Part A:

667 Journal of Power and Energy 2013;227(4):528-542.

668 [16] Gupta R, Biswas A, Sharma KK, Comparative study of a three-bucket Savonius rotor with

669 a combined three-bucket Savonius-three-bladed Darrieus rotor. Renewable Energy 2008;33(9):

670 1974-1981.

671 [17] Mertens S, van Kuik G, van Bussel G. Performance of an H-Darrieus in the Skewed Flow

672 on a Roof. Journal of Solar Energy Engineering 2003;125:433-440.

673 [18] Simão Ferreira CJ, van Bussel G, van Kuik G. An analytical method to predict the

674 variation in performance of a H-Darrieus in skewed flow and its experimental validation. Proc.

675 of the European Wind Energy Conference, February 27-March 2, 2006, Athens (Greece); 2006.

676 [19] Bianchini A, Ferrara G, Ferrari L, Magnani S, An improved model for the performance

677 estimation of an H-Darrieus wind turbine in skewed flow. Wind Engineering 2012;36(6):667-

678 686.

679 [20] Paraschivoiu I, Wind Turbine Design with Emphasis on Darrieus Concept. Polytechnic

680 International Press, Canada; 2002.

681 [21] Bianchini A, Ferrari L, Magnani S. Analysis of the Influence of Blade Design on the

682 Performance of an H-Darrieus Wind Turbine. Proc. ASME-ATI-UIT 2010 Conference on

683 Thermal and Environmental Issues in Energy Systems, Sorrento (Italy) May 16-18; 2010.

684 [22] Sharpe T, Proven G. Crossflex: Concept and early development of a true building

685 integrated wind turbine. Energy and Buildings 2010;42:2365-2375.

686 [23] Bianchini A, Ferrari L, Schneider A. First steps in the design and optimization of Darrieus

687 VAWTs for microeolic applications. Proc. World Renewable Energy Congress (WREC) X,

688 Glasgow (Scotland), July 19-25; 2008.

689 [24] Ferrari L, Bianchini A. Critical aspects in the design of a small-size Darrieus wind turbine.

690 Proc. World Renewable Energy Congress (WREC) XI, Abu Dhabi (UAE) September 25-30;

691 2010.

692 [25] Aslam Bhutta MM, Hayat N, Farooq AU, Ali Z, Jamil ShR, Hussain Z, Vertical axis wind

693 turbine – A review of various configurations and design techniques. Renewable and

694 Sustainable Energy Reviews 2012;16(4):1926-1939.

695 [26] Bianchini A, Ferrari L, Magnani S. Energy-yield-based optimization of an H-Darrieus

696 wind turbine. Proceedings of the ASME Turbo Expo 2012, Copenhagen (Denmark), June 11-

697 15; 2012.

698 [27] Manwell JF, McGowan JG, Rogers AL. Wind Energy Explained, 2nd edition, Wiley,

699 U.K.; 2009.

700 [28] Justus CG, Hargraves WR, Mikhail A, Graber D. Methods for estimating wind speed

701 frequency distributions. Journal of Applied Meteorology 1978;17(3):350-353.

702 [29] Akdağ SA, Dinler A. A new method to estimate Weibull parameters for wind energy

703 applications. Energy Conversion and Management 2009;50(7):1761-1766.

704 [30] Freitas de Andrade C, Maia Neto HF, Costa Rocha PA, Vieira da Silva ME. An efficiency

705 comparison of numerical methods for determining Weibull parameters for wind energy

706 applications: A new approach applied to the northeast region of Brazil. Energy Conversion and

707 Management 2014;86(10):801-808.

708 [31] Bhuyan S, Biswas A. Investigation on self-starting and performance characteristics of

709 simple h and hybrid H-Savonius vertical axis wind rotors. Energy Conversion and Management

710 2014;87:859-867.

711 [32] Gupta R, Das R, Sharma KK. Experimental study of a Savonius-Darrieus wind machine.

712 In Proceedings of the International Conference on Renewable Energy for Developing

713 Countries, University of Columbia, Washington DC, 2006.

714 [33] Bianchini A. Performance Analysis and Optimization of a Darrieus VAWT. PhD Thesis,

715 School of Energy Engineering and Innovative Industrial Technologies, University of Florence

716 (Italy); 2011.

717 [34] Islam M, Ting D, Fartaj A, Desirable Airfoil Features for Smaller-Capacity Straight-

718 Bladed VAWT. Wind Engineering 2007;31(3):165–196.

719 [35] Klimas PC. Tailored Airfoils for Vertical Axis Wind Turbines. Sandia National

720 Laboratories, Albuquerque, N.M., SAND 84-1062; 1984.

721 [36] Paraschivoiu I, Delclaux F. Double Multiple Streamtube Model with Recent

722 Improvements. Journal of Energy 1983;**7**(3):250-255.

723 [37] Balduzzi F, Bianchini A, Maleci R, Ferrara G, Ferrari L. Blade design criteria to

724 compensate the flow curvature effects in H-Darrieus wind turbines. Journal of Turbomachinery

725 2015;137(1):1-10.

726 [38] Camporeale SM, Magi V. Streamtube model for analysis of vertical axis variable pitch

727 turbine for marine currents energy conversion. Energy conversion and Management

728 2000;41(16):1811-1827

729 [39] Islam M, Ting D SK, Fartaj A. Aerodynamic models for Darrieus-type straight-bladed

730 vertical axis wind turbines. Renewable and Sustainable Energy Reviews 2008;12:1087-1109.

731 [40] Wang LB, Zhang L, Zeng ND. A potential flow 2-D vortex panel model: Applications to

732 vertical axis straight blade tidal turbine. Energy Conversion and Management 2007;4(2):454-

733 461.

734 [41] Simão Ferreira CJ. The near wake of the VAWT: 2D and 3D views of the VAWT

735 aerodynamics. PhD Thesis, Technische Universiteit Delft, The Netherlands, 2009.

736 [42] Bianchini A, Ferrari L, Magnani S. Start-up behavior of a three-bladed H-Darrieus

737 VAWT: experimental and numerical analysis. Proc. of the ASME Turbo Expo 2011,

738 Vancouver (Canada), June 6-10; 2011.

739 [43] Bianchini A, Ferrari L, Carnevale E.A.. A model to account for the Virtual Camber Effect

740 in the Performance Prediction of an H-Darrieus VAWT Using the Momentum Models. Wind

741 Engineering 2011;35(4):465-482.

742 [44] Ostowari C, Naik D. Post stall studies of untwisted varying aspect ratio blades with an

743 NACA 4415 airfoil section - Part I. Wind Engineering 1984;8(3):176-194.

744 [45] Dominy R, Lunt P, Bickerdyke A, Dominy J. Self-starting capability of a Darrieus turbine.

745 Proc. IMechE 221 Part A: Journal of Power and Energy 2007:111-120.

746

747

748

749

750

751

752

753

754

755

756
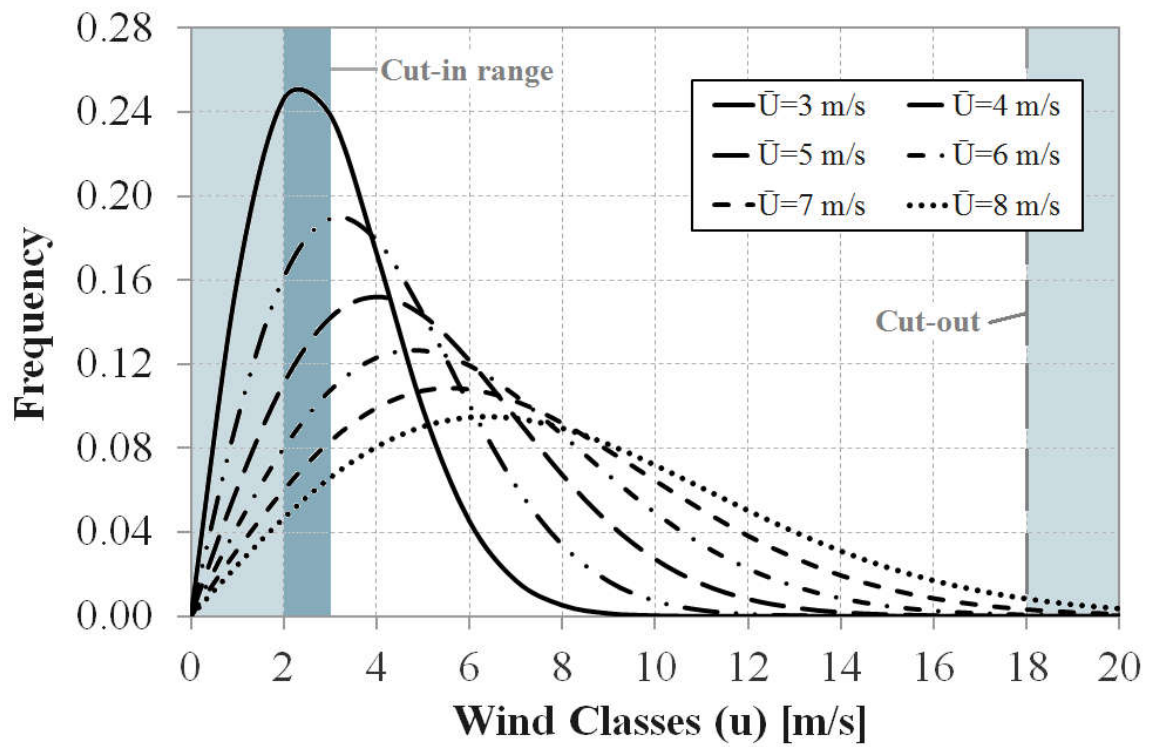
Legend:
- □ = Operating turbine
- ▨ = Turbine stopped
- ▨ = Start-up dependent on the configuration

757

strut

c

ω

A

H

D

758

NACA0018

Solid fillet

Stiffners

759

32

(a)

(b)

760

761

762

A=1 m²

A=4 m²

A=9 m²

NACA0015

σ	H
H/D	D
AR	c

765

766

767

768

769

36
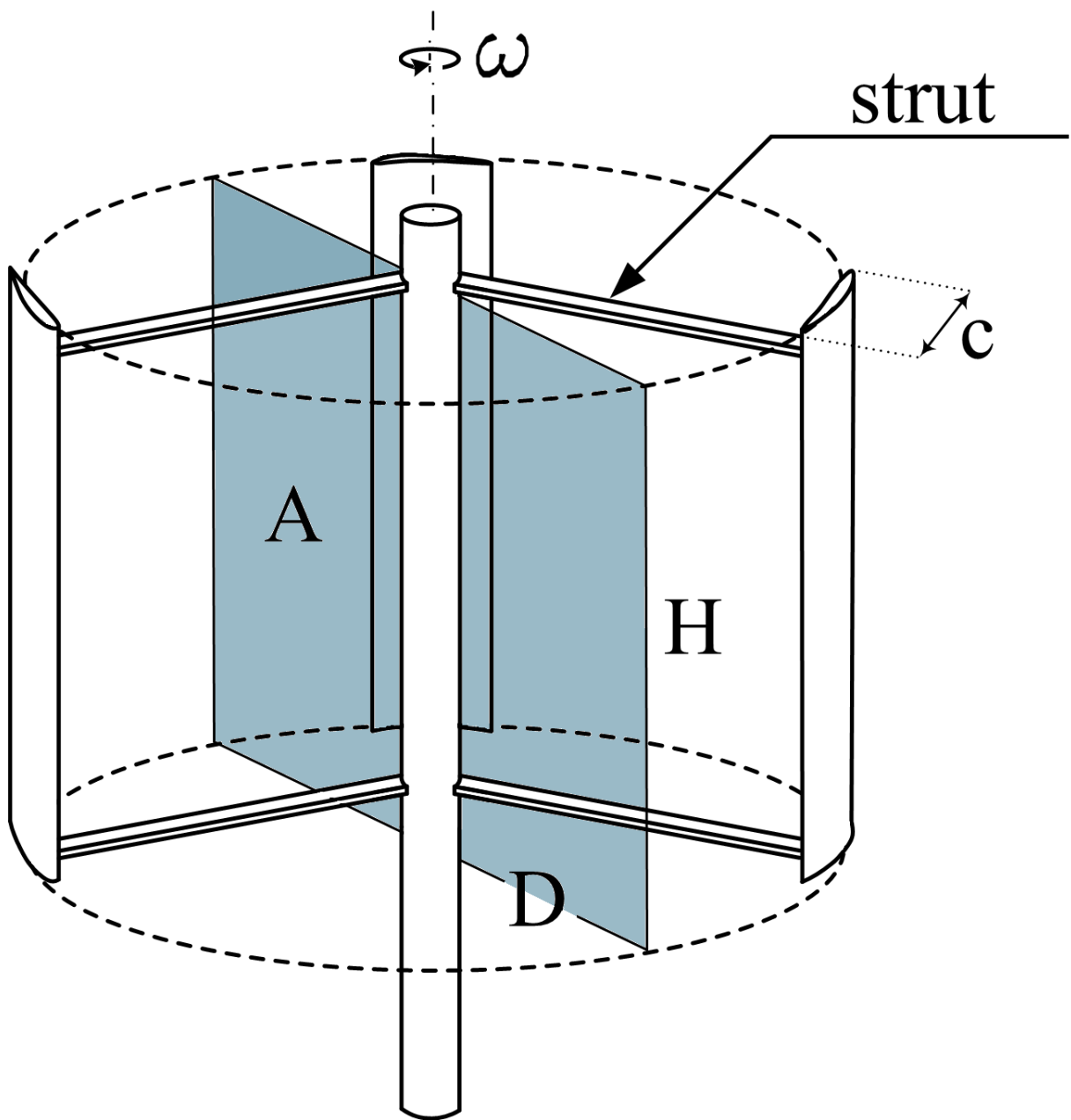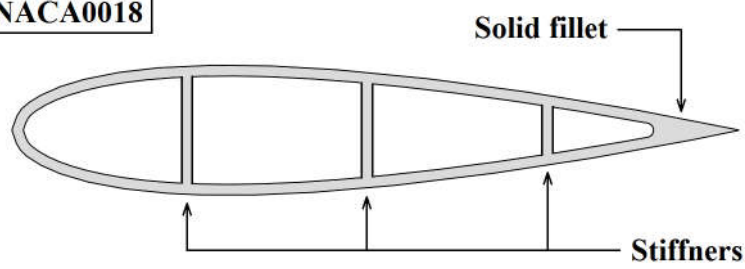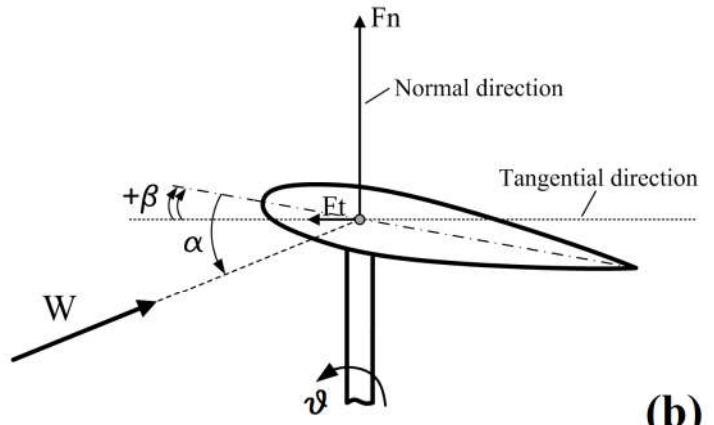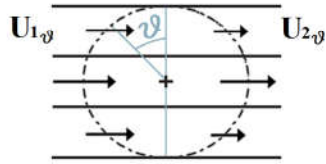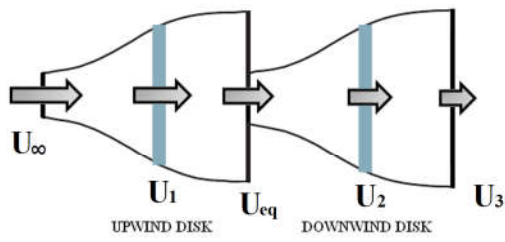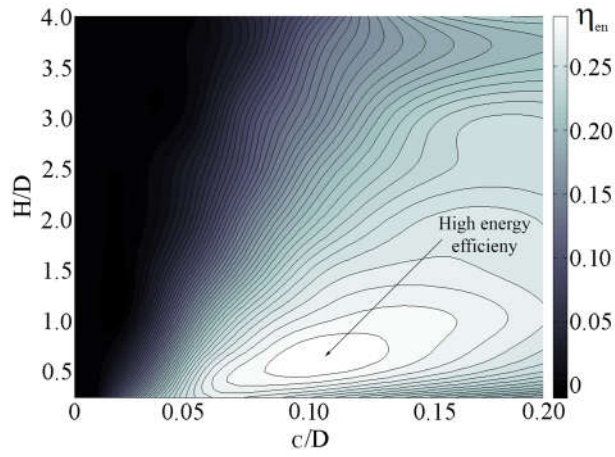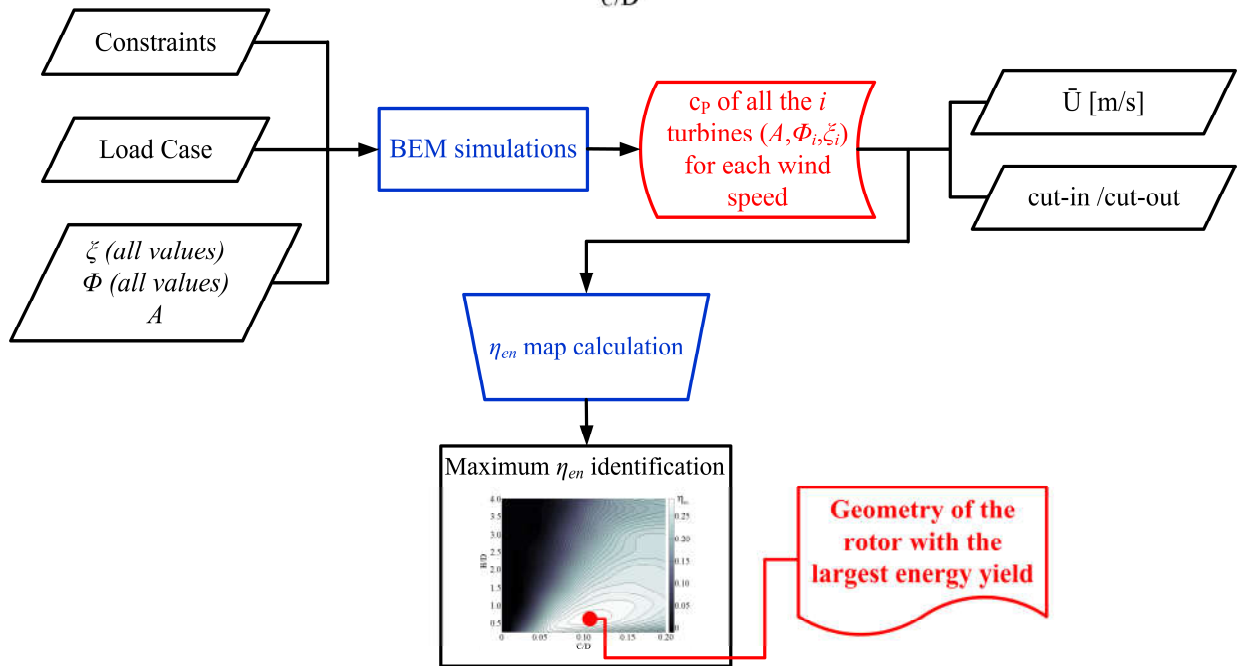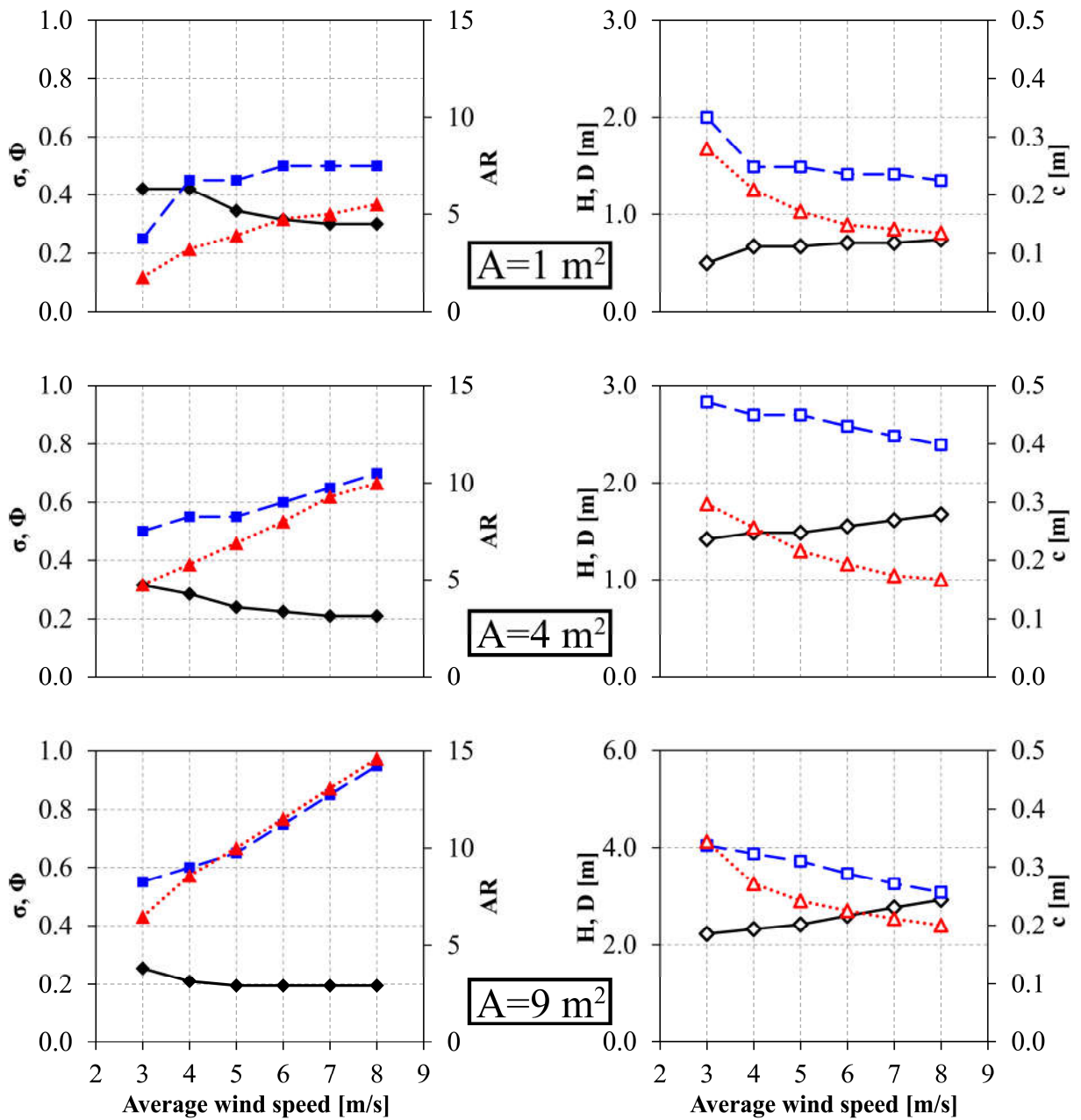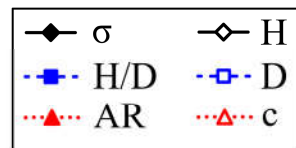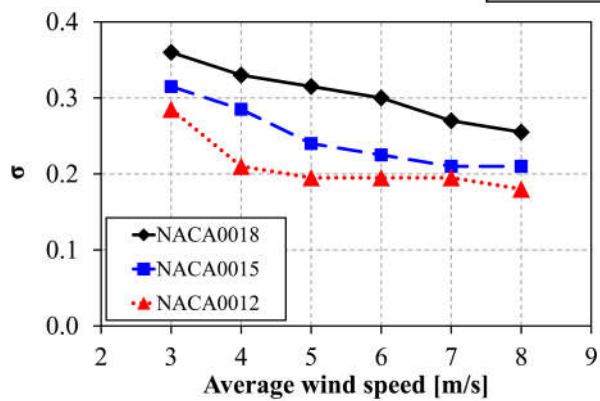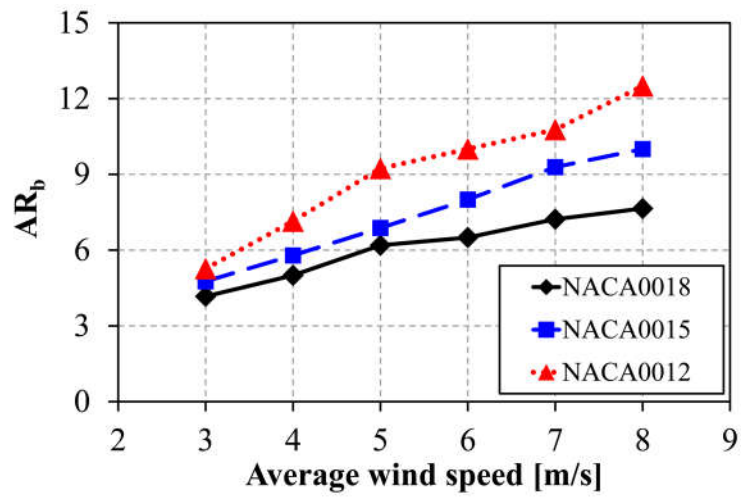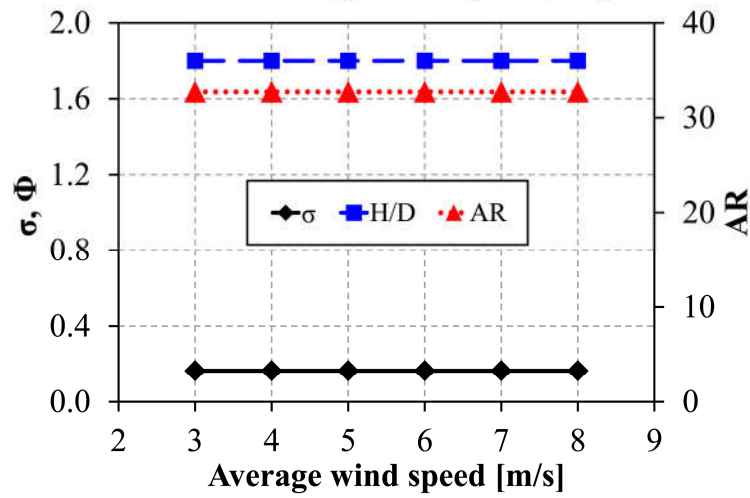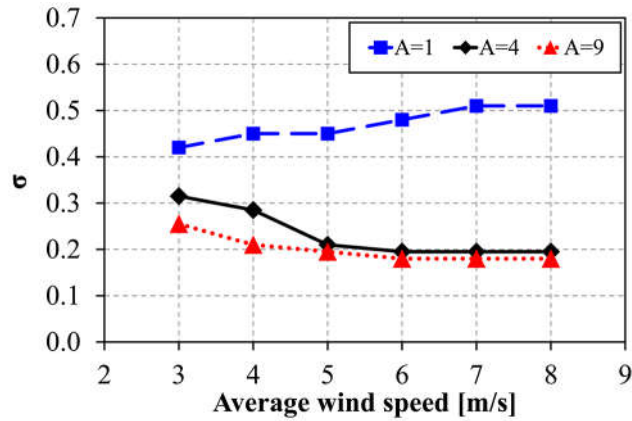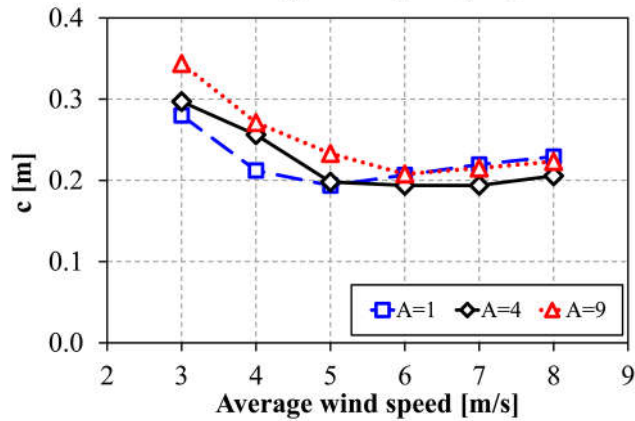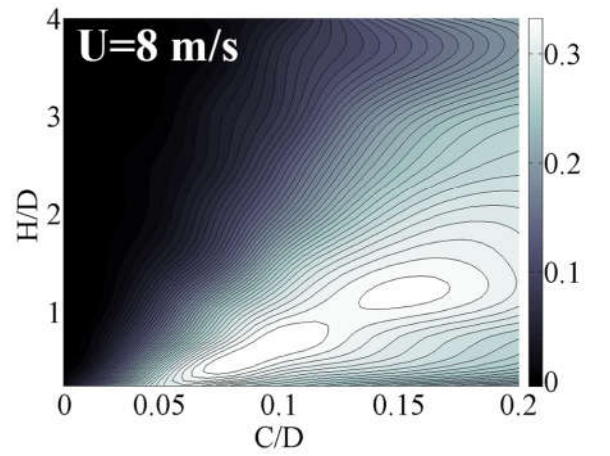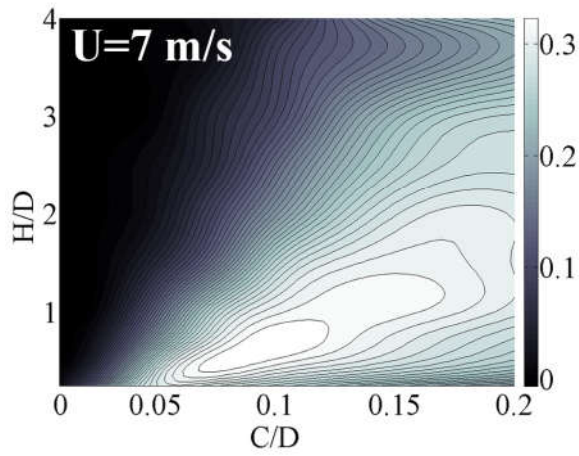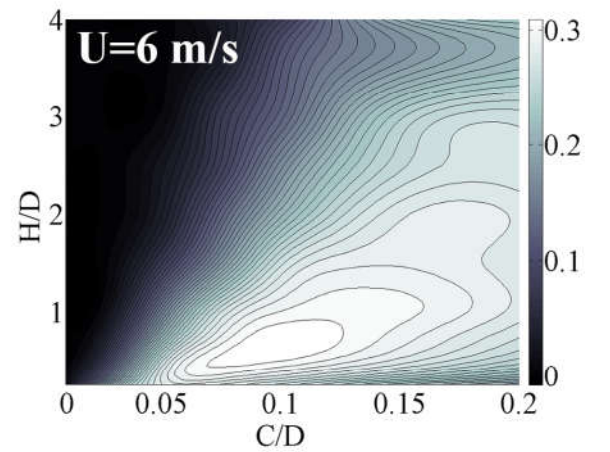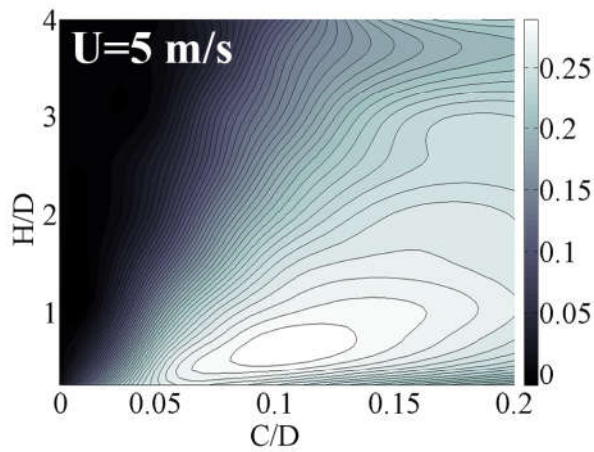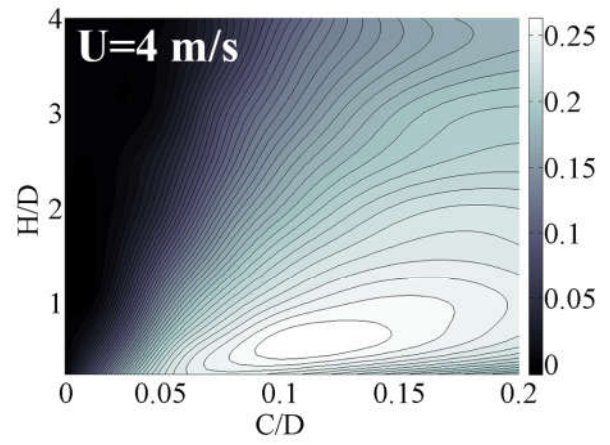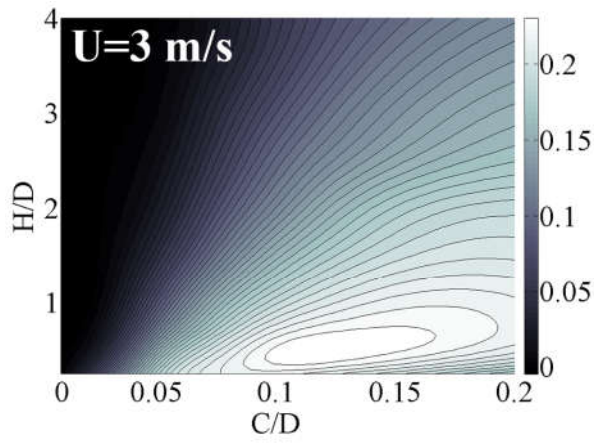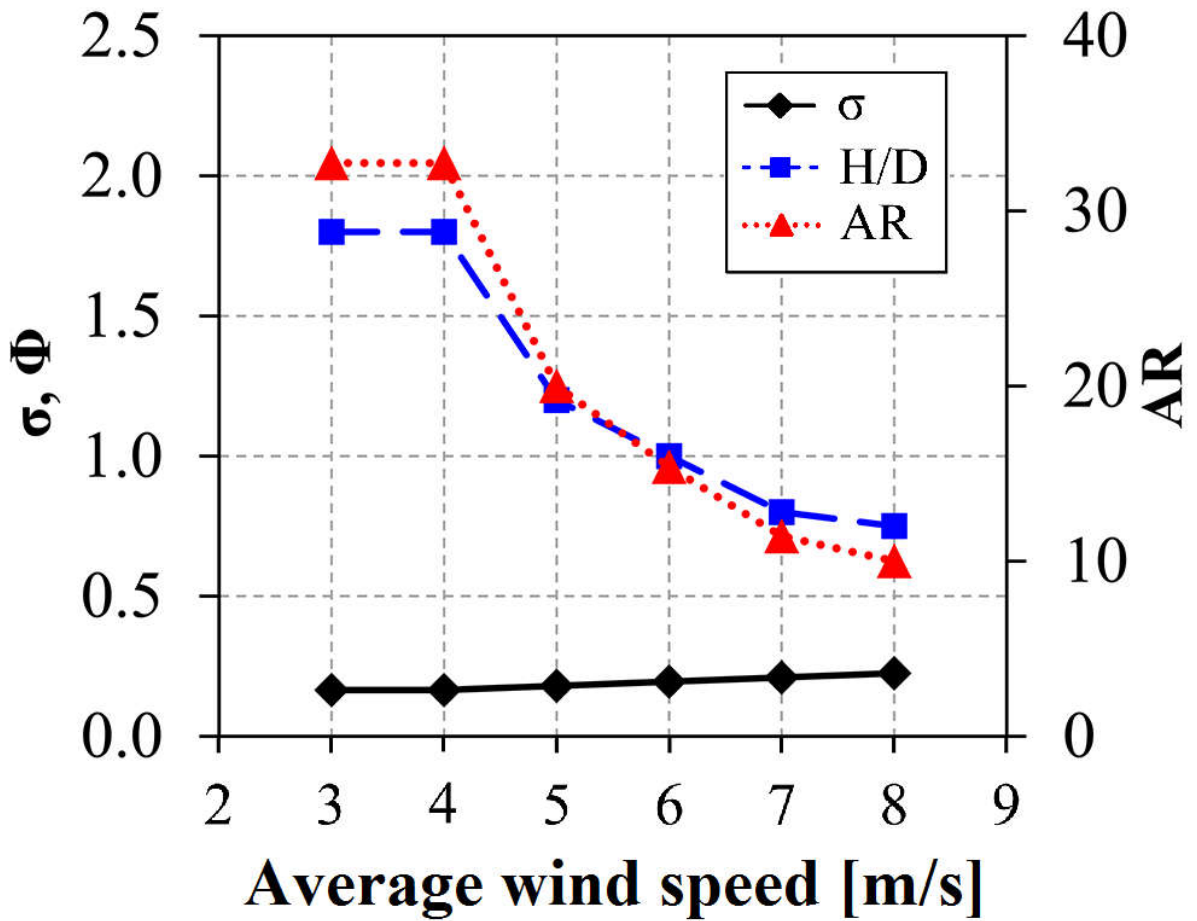
770

771

772

773

774

775

776